The application of particle image velocimetry for the analysis of high-speed craft hydrodynamics

Jacobi, Gunnar; Thill, Cornel; Huijsmans, Rene

Publication date
2016

Document Version
Final published version

Published in
Proceedings of the 12th International Conference on Hydrodynamics-ICHD 2016

THE APPLICATION OF PARTICLE IMAGE VELOCIMETRY FOR THE ANALYSIS OF HIGH-SPEED CRAFT HYDRODYNAMICS

G. Jacobi, C.H. Thill and R.H.M. Huijsmans
Department of Maritime and Transport Technology, Delft University of Technology
Mekelweg 2, 2628 CD Delft, The Netherlands
G.Jacobi@tudelft.nl, C.H.Thill@tudelft.nl, R.H.M.Huijsmans@tudelft.nl

ABSTRACT: The particle image velocimetry (PIV) technique has become a reliable method for capturing the velocity field and its derivatives, even in complex flows, and is now also widely used for validation of numerical codes. As the imaging system is sensitive to vibrations, the application in environments such as towing tanks makes it a challenging task. Especially when operating the towing tank carriage at higher speeds structural vibrations increase significantly. However, to apply this technique for the analysis of planing and semi-planing vessels, this is absolutely necessary. To assess the ability of a PIV system to capture the flow features close to a ship model while being towed at high speeds, a stereo PIV system was installed in the TU Delft towing tank. Measurements are conducted in the transom region of a generic high-speed vessel hull with a flat bottomed aft section, which is equipped with an interceptor at the transom. It is shown that with increasing carriage speed, vibrations of the imaging system increase, which ultimately can affect the quality of PIV recordings. The effect of vibrations is quantified by analysis of successive recordings and based on this, a shift correction is applied. A comparison with numerical results shows that the flow around the interceptor is well captured by the PIV system.

1. INTRODUCTION

As a result of the growing demand for high-speed vessels in coastal water and even offshore applications, and the need for these to operate in more challenging conditions, new concepts were developed in the recent years. While innovative hull shapes could improve the seakeeping behaviour over a broad range of conditions, also active motion control with the help additional appendages i.e. trim tabs and interceptors proved to reduce excessive motions allowing the ship to travel at higher speeds [1]. For performance prediction of these new concepts in the early design stage, reliable numerical tools are needed that can accurately model the characteristics of high-speed craft. To support this development towing tank tests are necessary to provide experimental data for validation purposes, but can be also seen as an alternative means to numerical methods. Especially the application of non intrusive measurement techniques such as particle image velocimetry (PIV) can give detailed insights into the flow field. It is increasingly employed for the analysis of hydrodynamics of ships in towing tanks environments and validation of numerical codes. Mostly applied for velocity measurments in the ship wake region [2], other applications range from manoevering [3] up to seakeeping related applications [4]. However, all reported experiments have been conducted at low Froude numbers for displacement vessels. As most actual imaging systems are attached to the towing tank carriage and towed next to the model through the water, the structure which accommodates the PIV system is exposed to structural vibrations which increase with increased towing velocity. Especially when high flexibility is needed, the cameras need to be able to be positioned independently from each other, without interacting hydrodynamically with the model and without influencing the flow in its vicinity.

To investigate the application of the PIV technique for the analysis of semi-planing and

planing vessels, a stereo PIV system is employed in the TU Delft towing tank. Two different setups are used to analyse the magnitude of the vibrations induced by structural vibrations of the carriage and the additional measurement error arising from these. To reduce the influence of vibrations, a correction method is applied which corrects for the shift between recorded images. Measurements are conducted in the transom region of a generic hull of a planing vessel with a flat bottom aft section. The transom of the model is equipped with an interceptor. When deployed at high speeds, the blade creates a stagnation region on the bottom of the hull in front of the transom, which is associated with a high pressure peak. Mainly used in static configurations the generated lift is used to influence the trim of a ship by dynamically changing the height of the interceptor, it is also used for active ride-control of fast ships in waves. The flow around interceptors is well analyzed and extensively described in literature [5]. Results from measurements in the center plane of the model will be compared to numerical results from CFD simulations.

2. EXPERIMENTAL SETUP

The PIV experiments were performed at the TU Delft towing tank no. 1. Its main dimensions are LxBxH 142 x 4.22 x 2.5 m with a maximum carriage speed up to 7 m/s. The model used for the measurements is a simplified planing hull shape with an aft segment with constant cross section of 0.8 m, overall length of l = 1.8m and width of b = 0.4 metres. The transom of the model was equipped with an interceptor of adjustable height. The interceptor is made from a flat plate, spanning the whole width of the model. The geometry was previously used by Rijkens et al. [1] who performed segmented model tests to assess the lift force generated by the interceptor. The bottom of the rectangular aft section was replaced with a perspex plate to provide optical access to the measurement area for illumination with the laser sheet. To accurately position the model with respect to the PIV system, the model was mounted to the carriage via a hexapod. Using a hexapod for traversing the model, made an extra traversing system for the PIV system redundant. While this system was also used for repositioning the model during a measurement, the measurements presented in this paper only describe measurements with a fixed model. However, the hexapod was used to lift the model out of the water at the end of

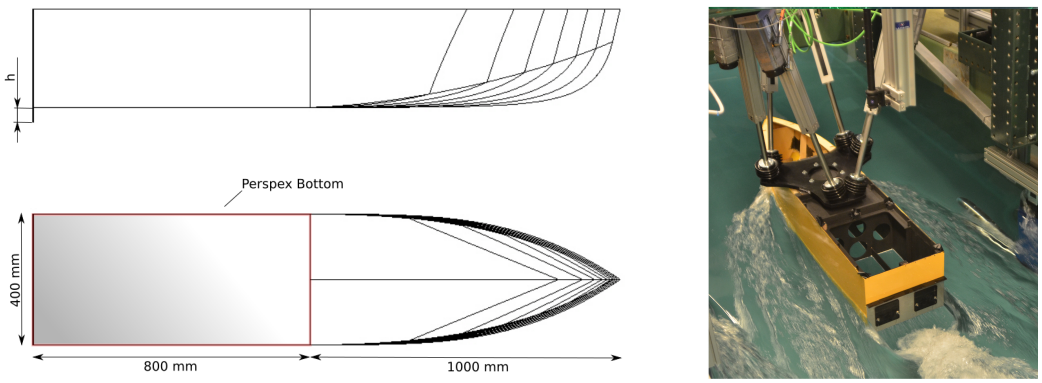

(a) (b)

Figure 1 - (a) Model geometry with main dimensions (b) Setup overview with laser-sheet optics and hexapod

each run, to prevent water from splashing into the model during deceleration of the carriage. The model geometry with its dimensions is depicted in Figure 1 a), while Figure 1 b) shows the hexapod and the position of the laser-sheet optics.

2.1 PIV Setup

PIV measurements are performed with two different underwater stereo-PIV setups, both with cameras located in separate housings to test the flexibility of positioning the cameras at various locations around the model. Both are depicted in Figure 2. In each case the laser head and optics were placed above the water and the field of view was illuminated through the perspex bottom of the model. To guarantee comparability between the setups, the laser optics were not moved in between tests. Each camera was placed in an underwater torpedo-shaped housing next to the model looking backwards to the measurement area with a 60° mirror section. Setup 1 is a symmetric setup with one camera on either side of the light sheet. With an angle of 90° between both cameras, highest accuracy is accomplished for the determination of the out of plane component. The immersion depth of the torpedoes is 500 mm and the cameras are located approx. 680 mm in front of the model's transom. Setup 2 is an asymmetric setup with the cameras on one side of the laser sheet, both looking backwards to the measurement area. While the longitudinal position of the camera remained the same, cameras were positioned 20 mm and 650 mm under the water surface, resulting in an angle of 25° between both cameras. Even if the cameras were positioned 650 mm in front of the transom, the length of the torpedo was chosen in such a way that the struts which connect the torpedo to the carriage are at the same longitudinal position as the transom of the model. To reduce the disturbance of the water surface through the struts, these have a streamlined shape. In both setups, the distance of all cameras is 1155 mm, measured from the centre of the measurement area.

For illumination of the measurement plane a 200 mJ Nd:YAG laser with a wave length of 532 nm was used. Operating in forward scattering mode, the laser power could be attenuated to 30 % of the total power with the use of the built in optical attenuator. Image recording was done with two scientific CCD cameras with a sensor size of 2448 x 2050 pixels. The pixel size is 3.45 x 3.45 μm and the frame rate is 15 Hz. The cameras were operated in double frame mode. They are equipped with 28 mm objectives resulting in a field of view of approximately 200 x

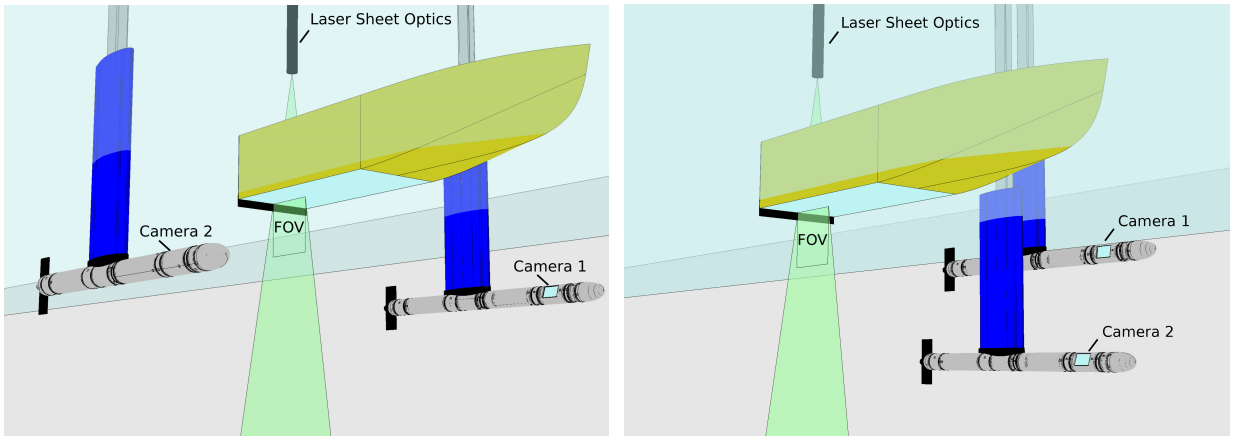

(a) (b)

Figure 2 - Stereo-PIV setup with camera arrangement and laser-sheet position: (a) Setup 1: Symmetrical setup (b) Setup 2: Asymmetrical setup

200 mm, with a digital resolution of 8 px/mm. In front of each camera a Scheimpflug-adapter was mounted to keep particles focused over the whole field of view. Seeding is done using 50 μm polymer (Vestosint) particles which were distributed with a seeding rake, mounted in the front of the carriage, in between runs.

3. PIV DATA PROCESSING

Data acquisition, as well as data post-processing was done using the commercial software package DaVis 8.3.0. The calculation of the velocity vector field is done in multiple correlation iterations. Starting with an interrogation window of 64x64 pixels in the initial pass, the window size was iteratively decreased to 24x24 pixels, using the vector field calculated in the previous pass for a window shift to ensure that the same particles are correlated with each other. The windows were overlapping by 50 % and a Gaussian weighting function was used.

While a complete discussion of measurement uncertainty exceeds the scope of this paper, one type should be shortly looked at to understand the postprocessing strategy: the registration error. It is typical for stereo-PIV applications and introduces the largest possible error. It occurs when the projected images from two different cameras do not match properly and velocity fields from different locations are used for vector calculation. Being extensively discussed in literature [6], it was first quantified by van Doorne et al. [7]. To test the misalignment of the recombined images from both cameras and correct for it Wieneke [8] proposed a method which is based on the cross correlation of two images, taken at the same instant of time. Using the resulting disparity map, calibration coefficients from an initial calibration can be corrected for a static misalignment. Assuming a laboratory environment, where light sheet and cameras do not move with respect to each other during the measurements, this method can completely correct for any disparity caused by a misalignment of laser sheet and calibration plate.

Operating a PIV system in a towing tank environment at high towing speeds, the system is prone to vibrations. Especially when cameras and light sheet optics are not rigidly connected, as it is the case with the two presented setups, a time varying disparity is expected. Calculating the disparity map for a sufficient number recordings a mean disparity between both cameras can be found to correct any initial misalignments of the images caused by a misalignment of laser sheet and calibration plate. As seen in Figure 3, which shows the mean calculated disparity after an initial misalignment correction for representative runs at 1 m/s and 5 m/s, a residual, time varying disparity is left. The increase of its amplitude with increasing carriage speed is

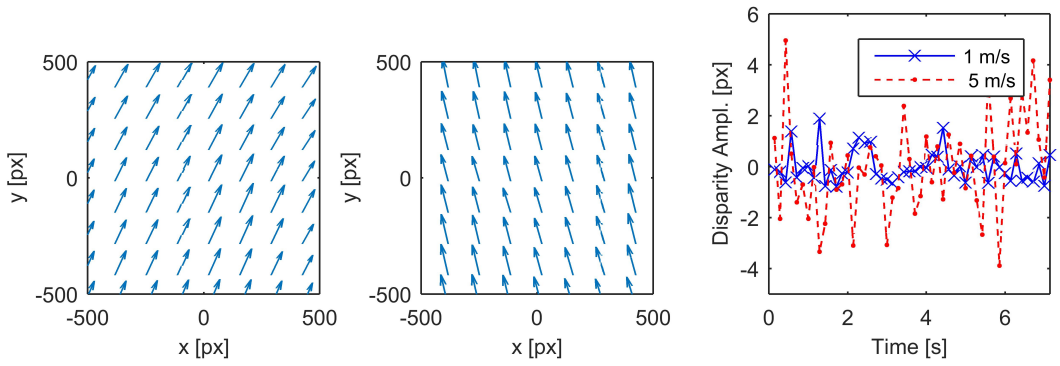

Figure 3 - Unsteady disparity vector field: (a) Instantaneous disparity vector field at two different instants of time (b) Unsteady disparity vector amplitude at 1 m/s and 5 m/s

attributed to the residual disparity that is caused by vibration of the PIV system. Considering the recommendation that displacement between particle pairs in dewarped images should not differ more than half the particle image size (2-3 pixels), a correction has to be applied to reduce the residual disparity between image pairs. Novara et al. [9], who performed multi-stereo-PIV measurements in a wind tunnel facility corrected the camera vibrations by cross-correlating each image pair of two cameras and correcting the camera mapping function for each time instant. Afterwards, they used a flow-feature based method to correct the shift between different stereo PIV systems. To eliminate the time varying shift of their velocity fields, they correlated the instantaneous velocity fields with a master velocity field. The resulting disparity vector was then used to correct the position.

The correction approach used in this paper is also based on a particle based correction and a feature based correction. However, instead of using a flow feature as a reference to correct for time varying shifts between the recordings, the ship bottom and the interceptor were chosen as a reference for correction. Observing both cameras separately, the first frame of each double image was cross-correlated with the first frame of the first image to calculate the shift relative to the master frame. The calculated shift vector was then used to perform a shift correction. Figure 4 a) shows the mean of the magnitude of the calculated shift vectors and their minimum and maximum values for both setups and speeds ranging from 1-5 m/s. For both setups a clear increase of vibration can be seen with increasing carriage speed. In the 5 m/s runs, single shift amplitudes up to 10 pixels could be detected, resulting in a possible range of 20 pixels. As this is the order of a correlation window, not applying the shift correction would strongly influence the results in regions with strong gradients. Having performed a shift correction for both cameras independently, the image sets from both cameras will still have a constant offset which is corrected by performing a second self-calibration, using the mean disparity vector field of all recordings. The result of the correction procedure can be seen in Figure 4 b), showing the RMS of the disparity magnitude before and after applying the shift correction. As already seen for the calculated camera shift, the initial magnitude of the disparity vector increases with speed. At 5 m/s the RMS of the deviation from the mean position is $\pm$ 4.5 pixels. After performing the two step correction deviation was reduced up to 0.7 pixel for the 1 m/s runs and a maximum of 2.5 pixels for the 5 m/s runs. Having only shown the influence of increasing speed on the pixel shift, the recognised pixel shift will also increase with the distance of the cameras from the field of view.

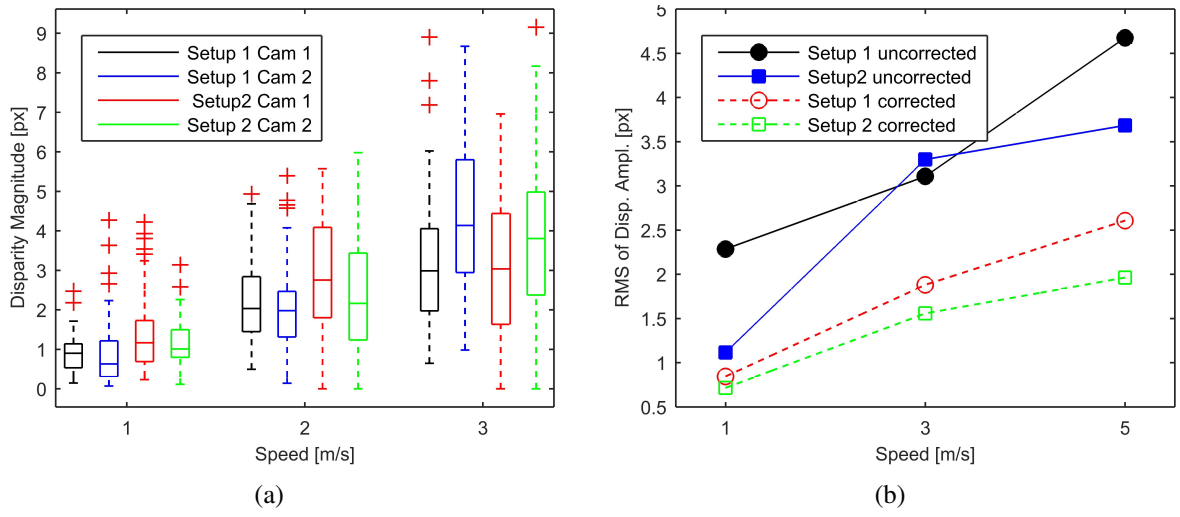

Figure 4 - (a) Determined image shifts (b) Initial Disparity and disparity after correction

4. NUMERICAL MODEL

For comparison with the measured PIV data, CFD simulations were performed at model scale on a 3D model with the open source code OpenFOAM. Using the interFOAM solver, the incompressible unsteady Reynolds-Averaged Navier-Stokes equations were solved while capturing the two-phase interface with the Volume of fluid (VOF) approach. For turbulence modeling, *k-ω-SST* model was applied. The governing equations are discretised with second-order schemes (central-differencing). The numerical grids are hexahedral unstructured meshes, generated with the software Hexpress. Assuming a symmetric flow, only one half of the model was meshed. The total dimensions of the grid are 8x1.1x1.3xLpp, while the cross section of the domain was chosen to fit the dimensions of the TU Delft towing tank. With additional refinements in the transom region, next to the interceptor position, the final mesh size was approximately 4 million cells. The simulations were performed at speeds ranging from 3 m/s to 5 m/s (Fn_L 0.71 to 1.18). For validation, the simulations are compared to model tests performed by Rijkens et al. [1], who used the same model geometry considered in this paper to analyse the generated lift and drag generated by an interceptor. As the model consisted of two separate segments, lift and drag force on the aft section could be measured. To prove that the influence of the interceptor on the flow is correctly modeled, lift forces measured during the segmented model test at different interceptor heights and speeds were compared to the lift force calculated from the CFD simulations. As seen in Figure 5 a) the effect of the interceptor is well modeled for all forward speeds and interceptor heights. The lift force generated by the interceptor is predicted with an average deviation of 5 %. Figure 5 b) gives an overview over the pressure distribution in the centre plane in longitudinal direction. The two peaks indicate the stagnation points at the bow and stagnation in front of the interceptor.

5. RESULTS

Before analysing the flow around an interceptor, the accuracy of the system is tested in open water conditions. As in this case, the laser sheet was guided through the perspex bottom of the

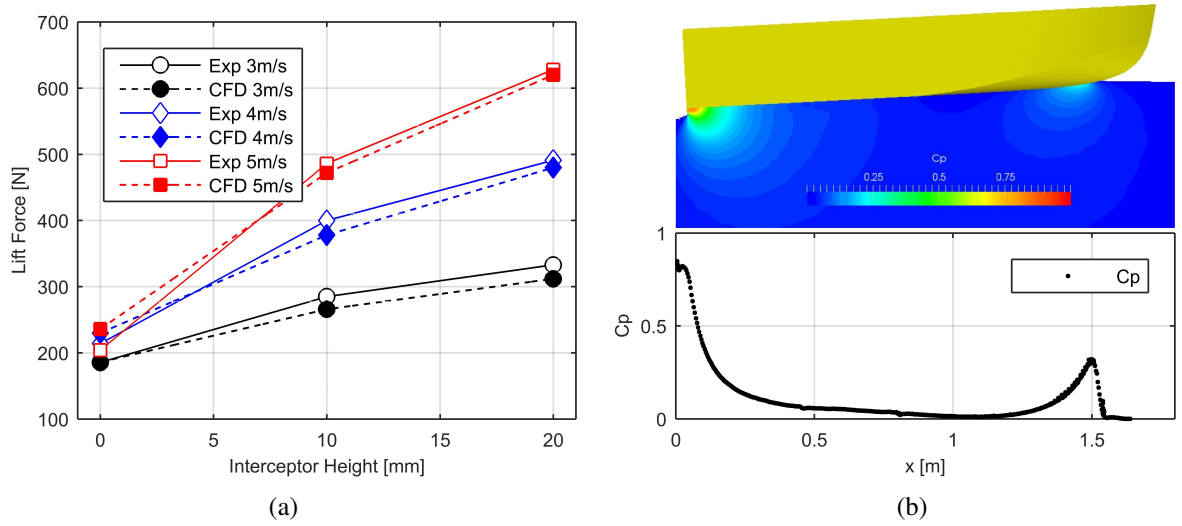

Figure 5 - (a) Comparison of measured and calculated Lift forces on aft section (b) Pressure distribution at the model's centre plane in longitudinal direction

model into the water, it was not possible to have full open water conditions. However, running the model with zero trim angle with reduced draft of 10 mm influence of the model on the flow was minimized and the velocity far away from the model assumed to be equal to the carriage speed. The test was performed with both setups at speeds ranging from 1 m/s up to 5 m/s. Both systems showed the same performance, deviating on average 3.5 % from the prescribed carriage speed. As an interceptor mainly influences the flow in the region next to the bottom of the model, the same reference runs were used to assess the measurement accuracy next to the bottom. The flat bottomed aft section of the model justifies a comparison of PIV measurements in the boundary layer to analytical results. Figure 6 shows the measured velocity magnitude averaged over 100 consecutive recordings and normalised by the free-stream velocity along the wall normal direction. Measurements are compared to semi-empirical power law velocity profiles of the form

$$u(\delta)/U_0 = (y/\delta)^{1/n}, \tag{1}$$

with $n = 7$. The turbulent boundary layer height δ was approximated according to Prandtl with

$$\delta \approx 0.37x/Re_x^{1/5} \tag{2}$$

Especially for 3 m/s and 5 m/s good agreement of the measurements with theory is found up to a distance of approx. half the correlation window size of 24 pixels. The deviations at 1 m/s might have been caused by the absence of turbulence generators on the model. These were intentionally not attached to the model, as the tests were designed to be conducted at higher speeds. Due to this the boundary layer might have been not fully developed. A visual inspection of the images shows a comparatively low seeding density near the wall in approx. 50 % of the recordings. In these pictures the flow is likely to be more laminar. For further analysis only speeds between 3 m/s and 5 m/s are considered.

To further assess the performance of the PIV system for capturing flow features close to the model at high towing velocities, measurements of test runs with interceptor heights of 10 mm and 20 mm are presented and compared to results from the previously described CFD calculations. Figure 7 shows an example of the averaged measured flow field calculated from 100 consecutive recordings. The interceptor height is 20 mm. The effect of the interceptor on the flow is well captured. The stagnation region is well pictured with a small recirculation zone in front of the interceptor. A more detailed comparison of the test runs is depicted in Figures 8

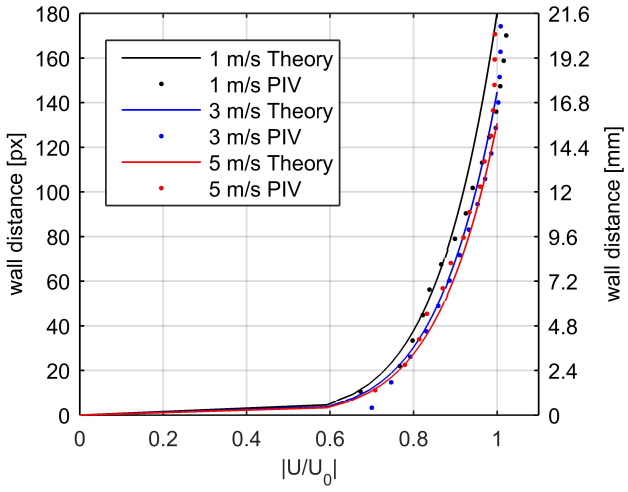

Figure 6 - Comparison of measured boundary layer profiles with semi-empirical profiles

and 9. These show the velocity profiles in wall normal direction, at different stations in front of the transom. The velocity is made dimensionless with the free-stream velocity U_0 and the wall distance is expressed relative to the interceptor height h.

The spacing of the stations in front of the interceptor was chosen to increase with decreasing pressure gradient. As can be seen, the effect of the interceptor is well captured for all cases. Due to the interceptor, the static pressure increases towards the transom, which results in an adverse pressure gradient. This results in a deceleration of the flow next to the bottom towards the transom. Measured and calculated velocity profiles match for all cases in the region down to 0.5*h. However, close the wall the flow is more strongly decelerated in the numerical solution, resulting in an early separation at x/h=4. In this study CFD calculations were deliberately chosen to be performed using wall functions to keep the computational costs at a low level. These may lead to the over prediction of the pressure gradient close to the boundary and thus leading to a separation of the flow. As the correlation window for both interceptor heights is 24 pixels, the resolution over the interceptor height was decreased by 50 % for the 10 mm case. However, the velocity profile in the boundary region is still well resolved. The same holds for the numerical results, as both grids had the same number of cells in wall normal direction.

6. CONCLUSION

To asses the ability of performing PIV measurements in a towing tank with high carriage speeds, a towed underwater stereo PIV system was installed in the TU Delft towing tank. Two different setups, with cameras mounted independently to the carriage, were utilised to picture the flow in the transom region of a planing hull that has an interceptor mounted to the transom. Structural vibrations of the towing tank carriage increased with increasing speed. The resulting unsteady displacement of the imaging system was quantified as a shift of the images in a series of recordings with respect to a reference image. At carriage speeds of 5 m/s images were shifted up to $\pm$10 pixels around their mean position. To reduce the registration error, the displacement, found from cross-correlation, was used as an input for a shift correction of these, reducing the initial disparity between images from both cameras to a maximum of 2.5 pixels. Given the fact, that

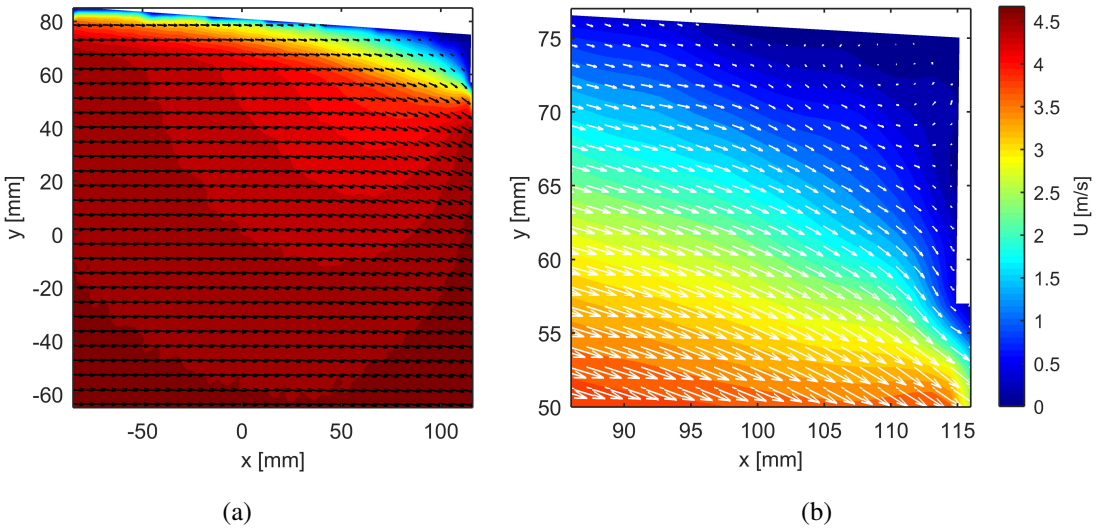

Figure 7 - Example of mean velocity contours and vectors calculated from 100 recordings (a) Overview over the whole field of view (b) Flow in front of the interceptor

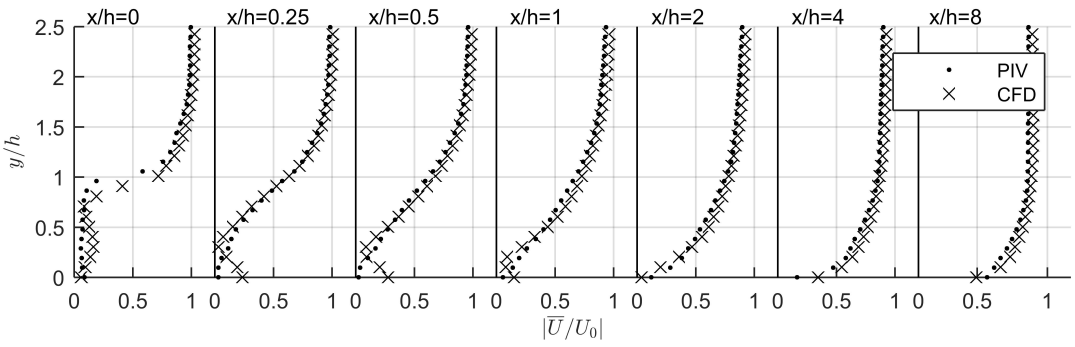

(a) 3 m/s

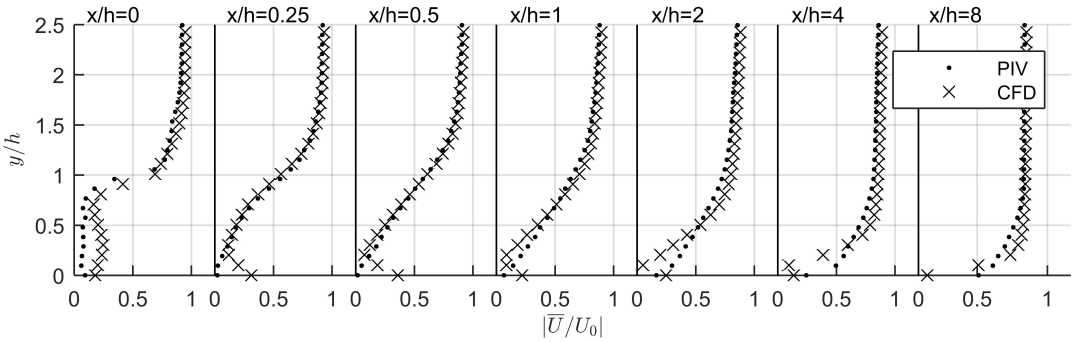

(b) 5 m/s

Figure 8 - Velocity profiles in wall normal direction at selected stations in front of the interceptor with h=20 mm at different speeds

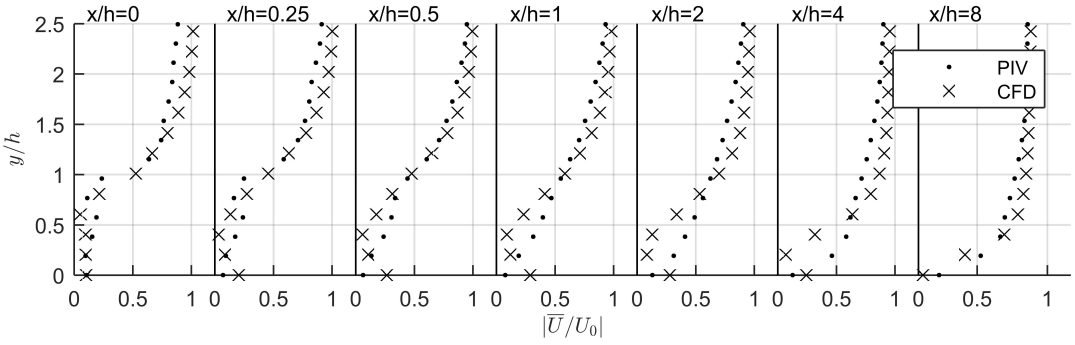

(a) 3 m/s

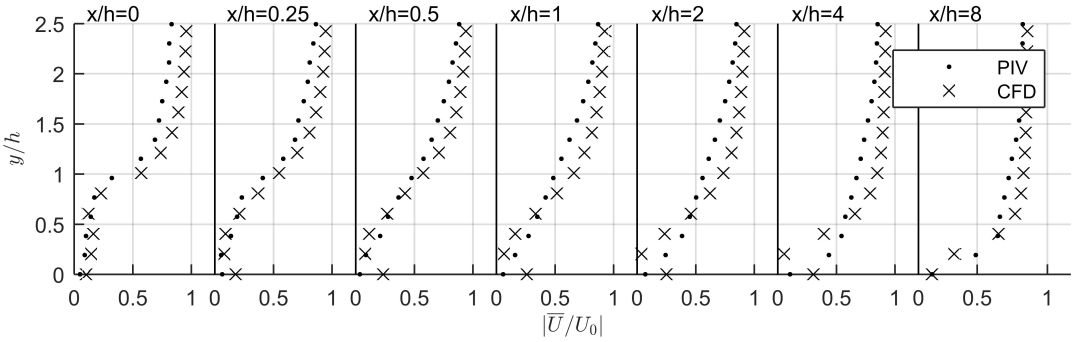

(b) 5 m/s

Figure 9 - Velocity profiles in wall normal direction at selected stations in front of the interceptor with h=10 mm at different speeds

the setup was not designed to fully resolve the boundary layer, but to capture the flow over a large distance along the model, the flow next to the hull is well resolved and captures the influence of the adverse pressure gradient that decelerates the fluid towards the transom. To further analyse the difference between measurements and CFD simulations in the near wall region, it is proposed to compare measurement data with wall resolved simulations, to avoid any influence of wall functions on the boundary layer flow.

7. REFERENCES

1. Rijkens, A. A. K. Cleijsen, H. M. A. Cleijsen, and Keuning, J. A. (2013) On the hydrodynamic performance of an improved motion control device for fast ships. *Proceedings of the 12th International Conference on Fast Sea Transportation*

2. Gui, L. and Longo, J. and Stern, F. (2001) Towing tank PIV measurement system, data and uncertainty assessment for DTMB Model 5512 *Experiments in Fluids* 31, 336-346

3. Falchi, M. and Felli, M. and Grizzi, S. and Aloisio, G. and Broglia, R. and Stern, F. (2014) SPIV measurements around the DELFT 372 catamaran in steady drift *Experiments in Fluids* 55, 18-44

4. Longo, J. and Shao, J. and Irvine, M. and Stern, F. (2007) Phase-Averaged PIV for the Nominal Wake of a Surface Ship in Regular Head Waves *Journal of Fluids Engineering* 5, 524

5. Brizzolara, S. (2003) Hydrodynamic analysis of interceptor with CFD methods *7th Int. Conference on Fast Sea Transportation - FAST* Ischia, Italy 2003 – Ischia, Italy

6. Prasad, A.K. (2000) Stereoscopic particle image velocimetry *Experiments in Fluids* 29, 103-116

7. Doorne, C.W.H. van, Westerweel, J. and Nieuwstadt, F.T.M. (2004) Measurement Uncertainty of Stereoscopic-PIV for Flow with Large Out-of-plane Motion *Particle Image Velocimetry: Recent Improvements: Proceedings of the EUROPIV 2 Workshop held in Zaragoza, Spain, March 31 - April 1, 2003* 213-227

8. Wieneke, B. (2005) Stereo-PIV using self-calibration on particle images *Experiments in Fluids* 39, 267–280

9. Novara M., Geisler, R. and Schröder, A. (2015) Multi-stereo PIV measurement of propeller wake flow in industrial facility *31st AIAA Aerodynamic Measurement Technology and Ground Testing Conference* Dallas